

A Climatology of Midlatitude Continental Clouds from the ARM SGP Central Facility. Part II: Cloud Fraction and Surface Radiative Forcing

XIQUAN DONG AND BAIKE XI

Department of Atmospheric Sciences, University of North Dakota, Grand Forks, North Dakota

PATRICK MINNIS

NASA Langley Research Center, Hampton, Virginia

(Manuscript received 30 November 2004, in final form 27 September 2005)

ABSTRACT

Data collected at the Department of Energy Atmospheric Radiation Measurement (ARM) Southern Great Plains (SGP) Central Facility (SCF) are analyzed to determine the monthly and hourly variations of cloud fraction and radiative forcing between January 1997 and December 2002. Cloud fractions are estimated for total cloud cover and for single-layered low (0–3 km), middle (3–6 km), and high clouds (>6 km) using ARM SCF ground-based paired lidar–radar measurements. Shortwave (SW) and longwave (LW) fluxes are derived from up- and down-looking standard precision spectral pyranometers and precision infrared radiometer measurements with uncertainties of $\sim 10 \text{ W m}^{-2}$. The annual averages of total and single-layered low-, middle-, and high-cloud fractions are 0.49, 0.11, 0.03, and 0.17, respectively. Both total- and low-cloud amounts peak during January and February and reach a minimum during July and August; high clouds occur more frequently than other types of clouds with a peak in summer. The average annual downwelling surface SW fluxes for total and low clouds (151 and 138 W m^{-2} , respectively) are less than those under middle and high clouds (188 and 201 W m^{-2} , respectively), but the downwelling LW fluxes (349 and 356 W m^{-2}) underneath total and low clouds are greater than those from middle and high clouds (337 and 333 W m^{-2}). Low clouds produce the largest LW warming (55 W m^{-2}) and SW cooling (-91 W m^{-2}) effects with maximum and minimum absolute values in spring and summer, respectively. High clouds have the smallest LW warming (17 W m^{-2}) and SW cooling (-37 W m^{-2}) effects at the surface. All-sky SW cloud radiative forcing (CRF) decreases and LW CRF increases with increasing cloud fraction with mean slopes of -0.984 and $0.616 \text{ W m}^{-2} \%^{-1}$, respectively. Over the entire diurnal cycle, clouds deplete the amount of surface insolation more than they add to the downwelling LW flux. The calculated CRFs do not appear to be significantly affected by uncertainties in data sampling and clear-sky screening. Traditionally, cloud radiative forcing includes not only the radiative impact of the hydrometeors, but also the changes in the environment. Taken together over the ARM SCF, changes in humidity and surface albedo between clear and cloudy conditions offset $\sim 20\%$ of the NET radiative forcing caused by the cloud hydrometeors alone. Variations in water vapor, on average, account for 10% and 83% of the SW and LW CRFs, respectively, in total cloud cover conditions. The error analysis further reveals that the cloud hydrometeors dominate the SW CRF, while water vapor changes are most important for LW flux changes in cloudy skies. Similar studies over other locales are encouraged where water and surface albedo changes from clear to cloudy conditions may be much different than observed over the ARM SCF.

1. Introduction

Clouds have been classified as the highest priority in climate change by the U.S. Climate Change Research Initiative (USCCRI 2001) because they are one of the

largest sources of uncertainty in predicting potential future climate change (Wielicki et al. 1995; Houghton et al. 2001). Clouds are the dominant modulators of radiation both at the surface and at the top of the atmosphere (TOA). Their impact on the earth's radiation budget is often represented via bulk cloud properties such as cloud amount, height, and microphysical/optical features (Wielicki et al. 1998; Curry et al. 2000; Houghton et al. 2001). Characterizing cloud effects on the surface radiation budget is a critical component for un-

Corresponding author address: Dr. Xiquan Dong, Department of Atmospheric Sciences, University of North Dakota, 4149 Campus Road, Box 9006, Grand Forks, ND 58202-9006.
E-mail: dong@aero.und.edu

derstanding the current climate and an important step toward simulating potential climate change.

Cloud radiative forcing (CRF; W m^{-2}), the change in the net radiation budget due to clouds (Ramanathan et al. 1989), represents the bulk effects of clouds on the radiation budget. CRF is a simple but effective means of studying cloud–radiation interactions and diagnosing problems in general circulation models (GCMs). The bulk effects of clouds are the integrated effects of individual cloud properties, which should be accurately parameterized in GCMs to correctly simulate atmospheric processes. These bulk effects constitute a first-order criterion for validating GCMs and improving their cloud parameterizations. For instance, by comparing with TOA radiative flux measurements, Cess et al. (1990) determined that the positive cloud feedback in some GCMs was too large. The feedbacks in those GCMs were reduced by altering the cloud optical properties in the parameterizations (Cess et al. 1996). The TOA CRF, however, represents only one component of the bulk effects of clouds. The surface CRF represents the other atmospheric energy boundary necessary to constrain the GCM parameterizations because the difference between the forcing at the TOA and the surface represents the cloud forcing within the atmosphere. Proper partitioning of the cloud radiative impact between the surface and the atmosphere is essential for assessing and modeling the effects of clouds on climate.

In the last few decades, our knowledge of the radiation budget at the TOA has been improved substantially with the advent of satellite observations from the Earth Radiation Budget Experiment (ERBE; see Barkstrom 1984) of the 1980s to the recent Clouds and the Earth's Radiant Energy System (CERES; see Wielicki et al. 1998). Satellite-derived TOA CRFs, reported as all-sky CRFs (i.e., the difference between net radiative fluxes for clear scenes and for all scenes including clear and cloudy conditions) yield a global net cooling of about -17 W m^{-2} for the earth–atmosphere system with the strongest cooling effect occurring in the middle latitudes (Ramanathan et al. 1989). Furthermore, low-level stratiform clouds were identified to have a strong net cooling effect while thin cirrus clouds appear to have a net warming impact on the earth–atmosphere system.

Progress has also been made in the development of global climatologies of the radiation budgets in the atmosphere and at the surface from limited long-term ground-based measurements. A relatively sparse surface radiation network has led to the extensive use of satellite data to estimate the surface radiation budget (SRB). The Global Energy and Water Cycle Experiment (GEWEX) SRB project was established in the

late 1980s to retrieve the SRB at all locations using operational satellite measurements. Several research groups have attempted to estimate surface radiative fluxes based on a variety of empirical parameterizations derived from radiative transfer model calculations, surface measurements, and satellite observations. These parameterizations have used ERBE broadband radiation data (Li and Leighton 1993; Tian and Ramanathan 2002), cloud data from the International Satellite Cloud Climatology Project (ISCCP; Zhang et al. 1995; Rossow and Zhang 1995), narrowband spectral radiances from the Geostationary Operational Environmental Satellite (GOES; see Gautier and Landsfeld 1997), and combinations of CERES cloud data and broadband fluxes (e.g., Charlock et al. 2003; Gupta et al. 2004). Comparisons of the satellite-derived surface radiation fluxes with the available surface measurements are generally in good agreement, but some of the differences in older datasets approach 50 W m^{-2} (e.g., Li and Leighton 1993). Comparisons between modeled and observed coincident surface and TOA fluxes during the 1990s, however, revealed large uncertainties in the modeling of the cloudy-sky shortwave (SW) radiation budget (e.g., Cess et al. 1995). Improvements in data reduction methods and radiative transfer models appear to have reduced the discrepancies to less than 10% (e.g., Ackerman et al. 2003).

Despite these advances in measuring, modeling, and inferring the surface radiation budget, there has been minimal progress in understanding and quantifying the relationships between cloud types and the surface CRF because clouds have not been quantified very precisely from the surface on a regular basis until recently. During the last decade, accurate measurements of cloud parameters have been taken simultaneously with radiation measurements on a nearly continuous basis at several surface sites operated by the Department of Energy Atmospheric Radiation Measurement (ARM; see Ackerman and Stokes 2003) Program. These new datasets make it possible to explore, in detail, the CRF at the surface and how it varies with cloud type, season, and time of day.

In a series of papers, we are developing a climatology of midlatitude continental cloud properties and their impact on the surface radiation budget using data collected at the ARM Southern Great Plains (SGP) Central Facility (SCF; 36.6°N , 97.5°W) from January 1997 to December 2002. Dong et al. (2005, hereafter Part I) generated a record of single-layer and overcast low-level stratus cloud macrophysical, microphysical, and radiative properties, and developed a new conceptual model of midlatitude continental low clouds. Here in Part II, we rely entirely on a combination of radar and

lidar/ceilometer measurements to identify clear sky, total cloud cover, and single-layered low, middle, and high clouds first and then calculate their corresponding CRFs. The present work, which uses the first nearly continuous set of long-term ground-based radiation and comprehensive cloud observations, should provide the most reliable estimates, to date, of monthly and hourly variations of cloud fractions and the impact of different clouds on the surface radiation budget. The results should be valuable for advancing our understanding of the cloud–radiation interactions and for enabling climate/forecast modelers to more fully evaluate their simulations over the SCF.

2. Data and analysis methods

The datasets (5-min resolution) in this study were collected directly or derived from surface measurements. The centerpiece of the cloud instrument array is the millimeter-wavelength cloud radar (MMCR; Moran et al. 1998). The MMCR operates at a wavelength of 8 mm in a vertically pointing mode and provides continuous profiles of radar reflectivity from hydrometeors moving through the radar field of view, allowing the identification of clear and cloudy conditions. Cloud-top height (Z_{top}) is derived from MMCR reflectivity profiles with an uncertainty of 45 m. Cloud-base height (Z_{base}) is derived from a composite of Belfort laser ceilometer, micropluse lidar (MPL), and MMCR data (Clothiaux et al. 2000). The laser ceilometer and lidar are sensitive to the second moment of the particle distribution (or the cross-sectional area of the particle), unlike the MMCR, which is sensitive to the sixth moment (it detects precipitation-sized particles, including insects, below cloud base). Thus, the ceilometer and lidar provide a more reliable estimate of cloud-base height than the MMCR. More details about the sensitivities and limitations of the cloud boundary products are available in Clothiaux et al. (2000).

The cloud fraction C is simply the percentage of returns that are cloudy within a specified sampling time period (e.g., month), that is, the ratio of the number of hours when both the radar and the lidar/ceilometer detected clouds to the total number of hours when all measurements were available (lidar/ceilometer and radar measurements and downwelling and upwelling SW and LW fluxes). This study uses $\sim 42\,214$ h for all-sky samples, which is 80.3% of all possible data during the 6-yr period. The total cloud fraction C_T is the fraction of time when a cloud is detected anywhere in the vertical column, the low cloud fraction C_L is the fraction of time when low clouds ($Z_{\text{top}} < 3$ km) occur without clouds above them, and the high cloud amount C_H is

determined for clouds having Z_{base} higher than 6 km with no clouds underneath, while middle clouds (C_M) range from 3 to 6 km without any clouds below and above. Although C_T , C_L , C_M , and C_H are computed using the same denominator (all-sky samples), C_T does not equal the sum of C_L , C_M , and C_H because C_T includes all cloudy conditions, such as some deep cumulus clouds and multilayered clouds that did not satisfy our definitions of single low-/middle-/high-cloud layers. These cloud fractions should not be confused with an instantaneous hemispheric cloud fraction observed by satellite observations and surface observers (Dong et al. 2005).

The SCF up- and down-looking standard Eppley Precision Spectral Pyranometers (PSPs) and Precision Infrared Pyrgeometers (PIRs) provide measurements of downwelling and upwelling broadband SW (0.3–3 μm) and longwave (LW, 4–50 μm) fluxes at the surface, respectively. In this study, the SW and LW fluxes are the Best Estimate Flux Value Added Products (VAP) from three different SCF radiometer systems: SIRS E13, C1, and Baseline Surface Radiation Network (BSRN), changed to Broadband Radiometer Station (BRS) in 2001, and their uncertainties are ~ 10 W m^{-2} (for more information, see Shi and Long 2002).

The CRF is the difference between the net surface fluxes (down–up) when clouds are present (Q_1 and F_1) and when they are absent (Q_0 and F_0 ; $C = 0$), and is defined as

$$\text{CRF}_{\text{SW}} = Q_1 - Q_0 \quad (1a)$$

and

$$\text{CRF}_{\text{LW}} = F_1 - F_0, \quad (1b)$$

respectively (Ramanathan et al. 1989; Dong and Mace 2003). The NET CRF, CRF_{NET} , is the sum of CRF_{SW} and CRF_{LW} at the surface. All-sky CRF refers to the difference between the net fluxes averaged for all-sky conditions and for clear skies only. Positive values of CRF indicate surface warming and negative values denote cooling of the surface. Since cloud-base temperature is typically greater than the clear-sky effective atmospheric radiating temperature, CRF_{LW} is generally positive. The magnitude of CRF_{LW} is strongly dependent on cloud-base height (i.e., cloud-base temperature) and emissivity. Conversely, clouds reflect more insolation than clear sky, therefore, CRF_{SW} is always negative over long time averages or large spatial domains. The magnitude of CRF_{SW} cooling strongly depends on the cloud optical properties and fraction, and varies with season. In this study, we calculate the monthly mean clear-sky net SW and LW fluxes first and then compute the monthly mean net SW and LW fluxes under the conditions of all sky, total, and single-layered

low, middle, and high clouds. Finally, we determine their corresponding CRFs using (1).

To avoid the temporal sampling biases in calculating CRF, the SW and LW fluxes under different sky conditions were binned and averaged in 1-h intervals first, and then the monthly means were calculated from the average of the 24-h means for a given month during the 6-yr period, irrespective of year. Thus, each 24-h mean has been equally weighted in calculating the monthly CRF regardless of the number of 5-min samples per hour. All local times (sample hours) for different sky conditions were sampled during the 6-yr period. The minimum number of samples per hour, 18 (~ 1.5 h), occurred for middle clouds, while the number of samples for low, high, and total clouds is generally about a magnitude greater than that for middle clouds. Therefore, there are enough samples in each local hour for low, high, and total clouds during the 6-yr period. Meaningful statistics in middle clouds may be questionable. The hourly weighted method should provide more representative values than simply using 5-min samples in calculating the monthly CRF. For example, the monthly mean might be biased if there were more 5-min samples at local noon than during early morning or late afternoon. Since the CRF is calculated from the difference in net fluxes between cloudy and clear skies, the impact of the instrument calibration biases and measurement errors on the calculated CRFs is not significant, and the CRF uncertainties should be smaller than the uncertainty of the flux measurements ($\sim 10 \text{ W m}^{-2}$).

To minimize the impact of different fields of view from the radar and lidar/ceilometer (point views) and PSP (global, hemispheric views) instruments on clear-sky fluxes, the clear-sky periods were identified by radar–lidar data first and then screened by the ratio of the PSP-measured downwelling SW flux to the clear-sky downwelling SW flux that would be recorded by the PSP if no clouds were present. This clear-sky flux is estimated using the approach of Long and Ackerman (2000). The downward SW fluxes measured on the clear-sky days closest in time to the cloudy days are fitted as a function of solar zenith angle. The curve-fit values are then interpolated to the cloudy days to estimate clear-sky downward SW fluxes that would be observed under the assumption of constant aerosol optical depth during the time period.

3. Results and discussions

a. Monthly variations

The monthly variations of C_T , C_L , C_M , and C_H during the 6-yr period are illustrated in Fig. 1a. Both C_T and

C_L peak during January and February and reach a minimum during July and August, and then gradually increase from summer to winter. The monthly variation of C_H mirrors that of C_L with local maxima from May through August followed by a significant drop into September that coincides with a rise in C_L . Single-layered middle clouds occur least frequently and have a small maximum during September.

Monthly mean downwelling SW and LW fluxes are shown in Figs. 1b and 1c for clear sky, all sky, total, and single-layered low, middle, and high clouds, respectively. The mean downwelling SW flux extrema occur around the solstices with peaks during early summer and troughs during the December–January period. These patterns are primarily determined by seasonal changes in the intensity and duration of insolation and are only partially dependent on cloud fraction and optical properties. Maximum and minimum downwelling SW fluxes occur for clear skies and low clouds, respectively. Mean downwelling SW fluxes for other cloud types fall between that for clear skies and low clouds. Conversely, the relative magnitudes of the corresponding downwelling LW fluxes are opposite those for SW fluxes. As shown in Fig. 1c, low clouds and clear skies have the greatest and smallest downwelling LW fluxes, respectively. The monthly variations of cloudy downwelling LW fluxes are mainly governed by variations in cloud-base temperature (summer maxima and winter minima; Dong et al. 2005). Clear-sky values are primarily determined by the atmospheric temperature profile and precipitable water vapor (PWV) with winter–summer extrema (see section 4).

From the monthly means and annual averages in Fig. 1, we can classify these downwelling SW and LW fluxes into three groups: 1) clear sky with maximum SW and minimum LW fluxes, 2) total and low clouds with minimum SW and maximum LW fluxes, and 3) all-sky, and middle and high clouds with the values between groups 1 and 2. The monthly mean clear-sky SW and LW fluxes constitute the references herein for studying the impact of clouds on the SRB. As demonstrated in Fig. 1, cloudy downwelling LW fluxes are greater and SW fluxes are smaller than those for clear skies. The downwelling LW fluxes for clouds are primarily determined by cloud height (temperature) and microphysical properties such as emissivity (e.g., Shupe and Intrieri 2004). High clouds with low cloud-base temperature and emissivity produce a small downwelling LW radiation, which is mostly absorbed by the abundance of atmospheric moisture before it arrives at the surface. Consequently, the high-cloud-emitted downwelling LW radiation at the surface is small and only slightly larger than the clear-sky value. The SW fluxes are less and

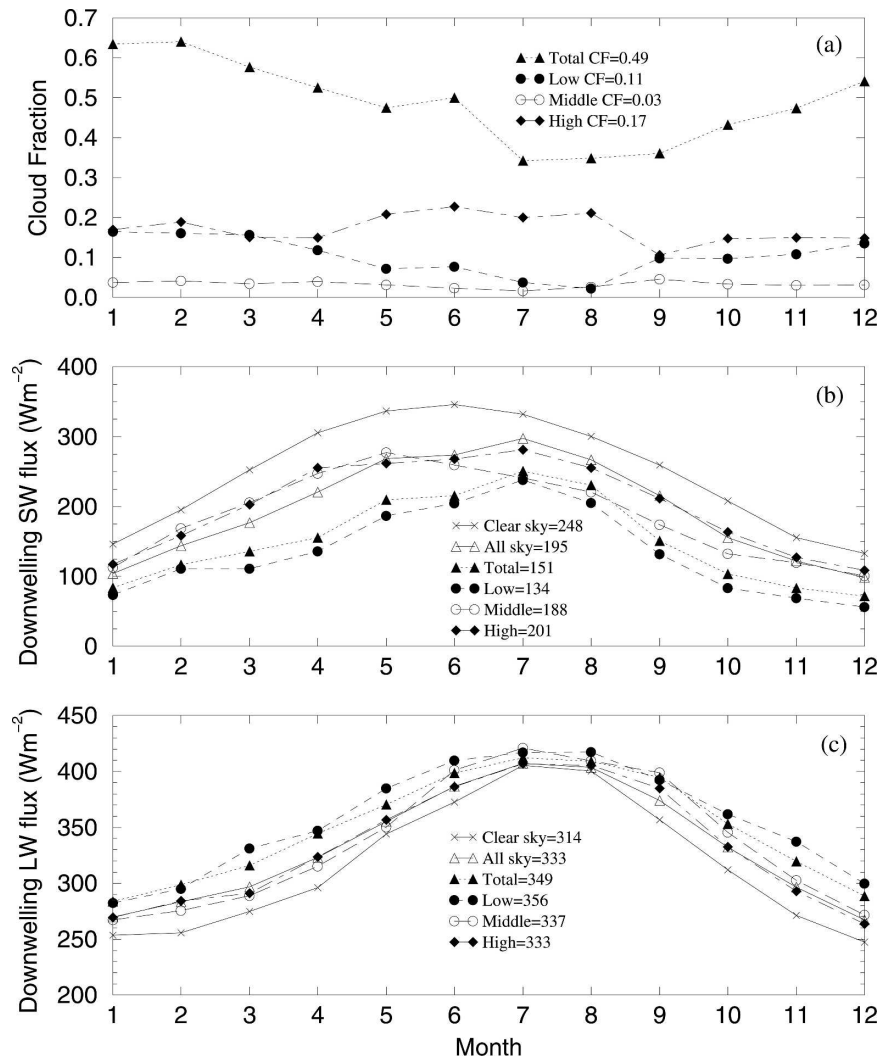


FIG. 1. Monthly mean radar–lidar-derived cloud fractions and observed downwelling fluxes at ARM SCF, 1997–2002. (a) Monthly mean total, and single-layered low- ($Z_t \leq 3$ km), middle- ($Z_b > 3$ km, $Z_t \leq 6$ km), and high- ($Z_t > 6$ km) cloud fractions C . Downwelling (b) SW and (c) LW fluxes measured by upward PSP and PIR.

LW fluxes are greater for total and low clouds than those for other cloud types throughout the whole year except during July and August. During that period, the monthly mean LW fluxes for total and low clouds are close to the clear-sky values, presumably because the large amounts of summertime water vapor (an effective emitter) make it difficult to “see” clouds in the LW. For SW flux, low clouds are optically thinner during that period (Dong et al. 2005). The LW radiative influence of the lowest clouds on the surface is minimized by absorption in the layer between the surface and cloud base.

For the most part, it can be inferred that total cloud cover is dominated by low clouds, either single-layered or multilayered systems with a significant low-cloud

component. In general, the SW and LW fluxes for C_T and C_L are close during all months, differing in the mean by 17 and 7 W m^{-2} , respectively. Furthermore, it can be inferred that the cloud optical depth is much greater for systems containing low clouds because the minimum SW fluxes occur for low and total clouds.

The LW and SW CRFs are governed primarily by the differences in downwelling LW and SW fluxes between cloudy and clear-sky conditions because the differences between their upwelling fluxes are minor relative to their downwelling counterparts. The monthly means of the LW, SW, and NET CRFs for all cloud types are illustrated in Fig. 2, and their seasonal means are summarized in Table 1. The total and low-cloud LW CRFs peak during spring and fall and bottom out during July

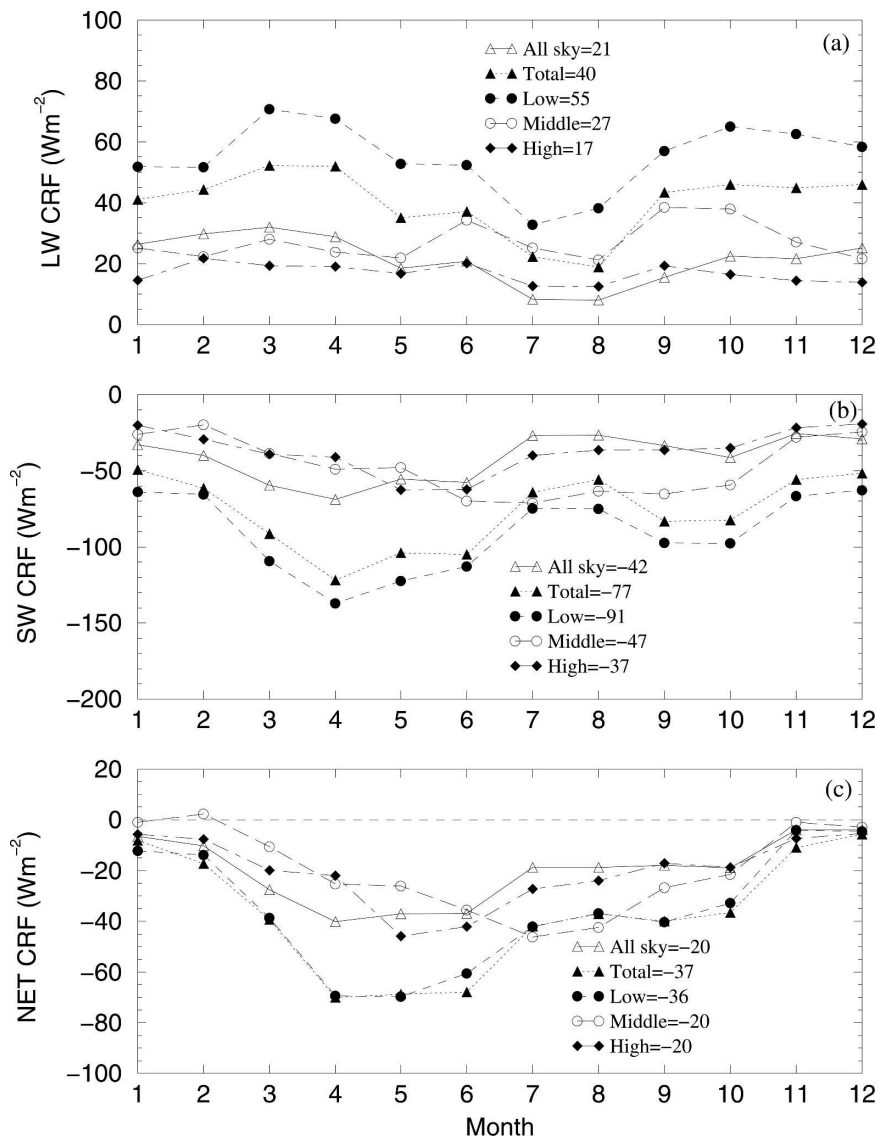


FIG. 2. Monthly mean CRF at ARM SCF, 1997–2002: (a) LW, (b) SW, and (c) NET.

and August, consistent with changes in the downwelling LW fluxes (Fig. 1c). The LW CRFs for all-sky middle and high clouds, as expected, are generally smaller than those for total and low clouds except the middle-cloud

LW CRFs, which are slightly larger than those for total clouds during the summer. The variations in SW CRFs almost mirror their LW counterparts. The SW CRFs for all-sky middle and high clouds are much less nega-

TABLE 1. Seasonal and annual averages of SW/LW/NET clear-sky flux and CRF at the ARM SCF. Units: $W m^{-2}$.

	Winter	Spring	Summer	Autumn	Annual
	SW/LW/NET	SW/LW/NET	SW/LW/NET	SW/LW/NET	SW/LW/NET
Clear sky	123.8/–85.3/38.6	238.5/–90.8/147.8	260.1/–74.1/186.0	164.8/–82.5/82.3	196.8/–83.1/113.7
All sky	–34.0/27.1/–6.9	–61.3/26.4/–34.9	–37.1/12.3/–24.8	–33.4/19.8/–13.6	–41.5/21.4/–20.1
Total cloud	–54.1/43.7/–10.4	–105.8/46.4/–59.4	–75.0/26.0/–49.0	–73.8/44.7/–29.2	–77.2/40.2/–37.0
Low cloud	–64.2/53.9/–10.3	–123.0/63.7/–59.3	–87.6/40.7/–46.9	–87.2/61.5/–25.8	–90.5/55.0/–35.5
Middle cloud	–23.5/23.0/–0.5	–45.2/24.5/–20.7	–68.2/26.8/–41.4	–50.9/34.4/–16.5	–47.0/27.2/–19.8
High cloud	–22.9/16.7/–6.3	–47.6/18.3/–29.3	–46.2/15.1/–31.1	–31.1/16.7/–14.4	–37.0/16.7/–20.3

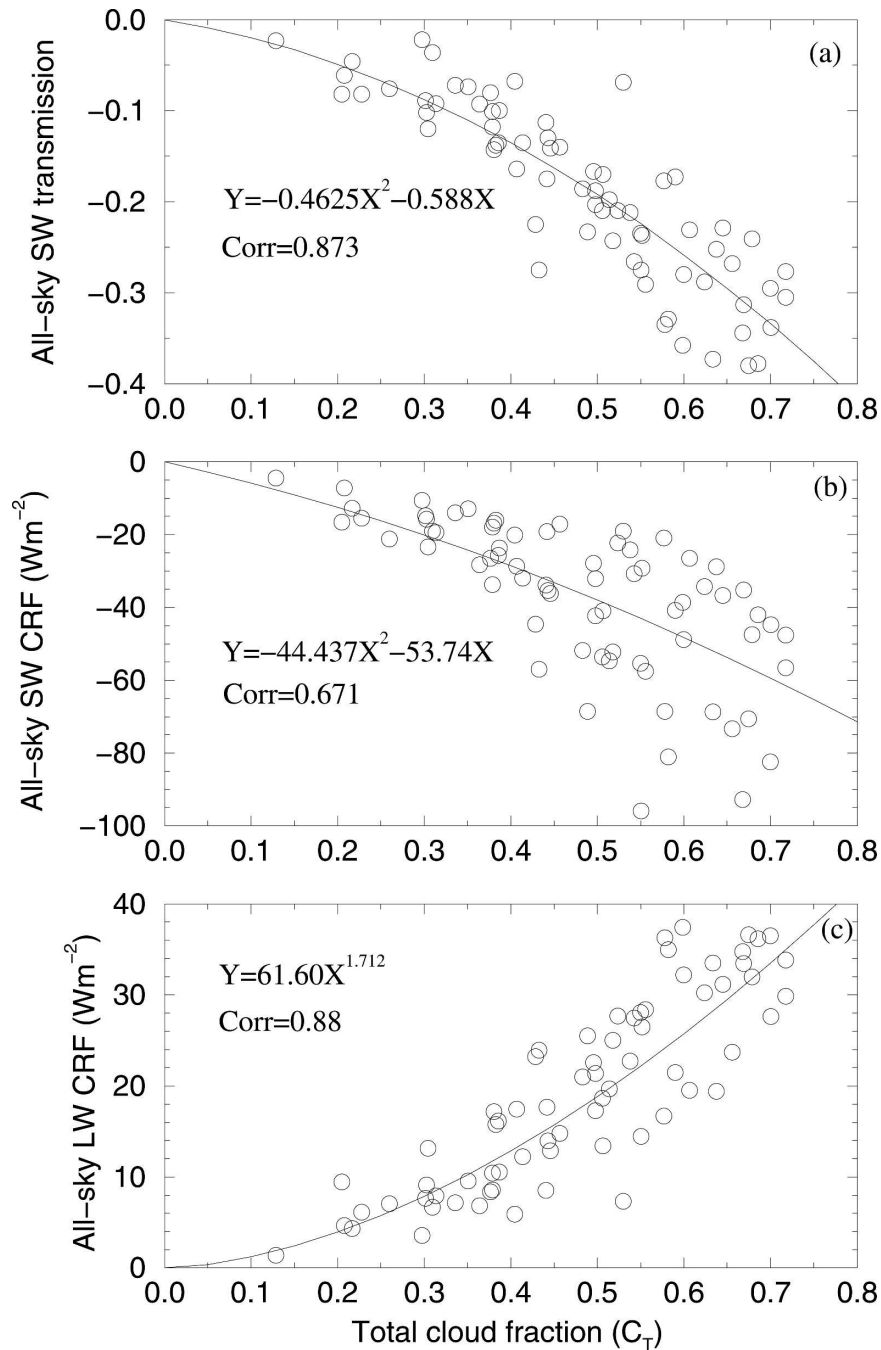


FIG. 3. Dependence of all-sky transmission and CRF on monthly mean cloud amount at ARM SCF, 1997–2002. Scatterplots and polynomial regression fits for monthly mean all-sky (a) SW transmission, and all-sky (b) SW and (c) LW CRFs.

tive than those for total and low clouds. NET CRFs, the sum of SW and LW CRFs, are primarily determined by SW CRFs throughout most of the year. During winter, however, the negative SW CRFs and positive LW CRFs nearly cancel each other, resulting in NET CRFs between -17 and $+2 \text{ W m}^{-2}$.

To quantify the impact of cloud amount on the SRB, the 72 ($6 \text{ yr} \times 12 \text{ month}$) monthly mean SW transmissions and SW and LW CRFs for all-sky conditions are plotted in Fig. 3 against their corresponding monthly mean total cloud fractions (C_T). All-sky SW transmission is defined as the ratio of the difference in mean

downwelling SW fluxes under all-sky and clear-sky conditions to the mean downwelling clear-sky fluxes. As illustrated in Fig. 3a, all-sky SW transmission decreases with increasing C_T . For example, when C_T increases by 0.01 or 1%, all-sky SW transmission decreases, on average, by 0.0059 or $\Delta T_{\text{SW}}/\Delta C_T \sim -0.59\%^{-1}$. The actual changes are asymptotic with respect to changes in C_T because, overall, the optical depths tend to increase with increasing cloud fraction. The divergence in the data for $C_T > 0.45$ suggests that a greater variety of cloud thicknesses occur as the cloud fraction increases. The sensitivity of all-sky SW CRFs to C_T is very similar to their transmission counterpart, that is, all-sky SW CRF decreases with increasing C_T with a slope of $-0.984 \text{ W m}^{-2} \%^{-1}$ or $\Delta \text{CRF}_{\text{SW}}/\Delta C_T \sim -0.984 \text{ W m}^{-2} \%^{-1}$ (in units of watts per squared meter per percent cloudiness). Conversely, all-sky LW CRFs increase with increasing C_T with a ratio of $0.616 \text{ W m}^{-2} \%^{-1}$. The net impact of cloud amount on the SRB should be the sum of SW and LW effects, that is, $\Delta \text{CRF}_{\text{NET}}/\Delta C_T = \Delta \text{CRF}_{\text{SW}}/\Delta C_T + \Delta \text{CRF}_{\text{LW}}/\Delta C_T = -0.368 \text{ W m}^{-2} \%^{-1}$.

The variations of mean SW transmission and CRF with C_T are only representative of the ARM SCF. The variations will depend on the cloud types and surface characteristics. For example, the sensitivity of CRF_{LW} to C_T in Fig. 3c is close to that observed by Shupe and Intrieri (2004), who used a year of the Surface Heat Budget of Arctic Ocean (SHEBA) dataset. However, the sensitivity of CRF_{SW} to changes C_T in Fig. 3b is much greater than that observed by Shupe and Intrieri (2004) because the surface albedo at the SCF is much smaller than over the Arctic ice pack. As mentioned earlier, CRF represents the bulk effects of clouds on the SRB via cloud optical depth and fraction, and seasonal variation. The relationships between all-sky SW transmission and SW and LW CRFs with C_T in Fig. 3 implicitly include cloud optical depth and solar zenith angle changes, which probably account for much of the scatter in the plots. A more comprehensive parameterization that includes cloud fraction and optical depth, solar zenith angle, and seasonal variation is beyond the scope of this study.

b. Diurnal cycle

The hourly mean cloud fractions and downwelling SW and LW fluxes from the 6-yr dataset are shown in Fig. 4 to determine the cloud diurnal cycles and their impact on the SRB over the SCF. More C_T and C_L occur in the morning and early afternoon than at late afternoon, C_H nearly mirrors those of C_T and C_L , and C_M is relatively invariant. It is clear that the low-cloud diurnal cycle is the most significant among the different cloud types.

The 6-yr hourly mean downwelling SW and LW fluxes for each scene type are illustrated in Figs. 4b and 4c, respectively. The relative magnitudes of the hourly means are the same as their monthly counterparts, that is, the maximum and minimum downwelling SW and LW fluxes occur in clear skies, and vice versa for low clouds, with fluxes for the other scene types between them. The insolation under each of the different sky conditions follows the solar zenith angle. The impact of clouds on the SRB is clearly demonstrated in Fig. 4. The total- and low-cloud insolation during the afternoon is noticeably larger than during the morning, which coincides with decreasing C_L and thinning low clouds during the afternoon (Dong et al. 2005). This behavior is similar to that of marine stratus, which typically thins out and breaks up during the afternoon (e.g., Minnis and Harrison 1984). The high-cloud insolation is only marginally smaller after noon than during the morning. The impact of total clouds on the SRB is most similar to that of low clouds, suggesting that the changes in C_L dominate the total-cloud diurnal cycle. In general, the mean fluxes change smoothly over the diurnal cycle. The fluctuations in middle-cloud downwelling SW and LW fluxes are a result of the limited number of samples. All downwelling LW fluxes are least in the early morning and greatest in the afternoon, consistent with the lower cloud-base heights and greater effective atmospheric radiating temperatures in the afternoon than in the early morning. It should be noted that the diurnal cycles in cloud amounts and fluxes presented here are for an average year. The mean diurnal cycle for an individual month can be much different than the annual mean.

Figure 5 shows the hourly mean clear-sky net (down-up) LW, SW, and NET fluxes and the corresponding CRFs for the different sky conditions. The annual mean clear-sky net LW flux (Fig. 5a) changes by only 70 W m^{-2} over the average 24-h period with a minimum (-129 W m^{-2}) at local noon and maxima (-59 W m^{-2}) from middle night to early morning. Despite the negative clear-sky NET flux during the nighttime hours, the daily NET flux is a positive (downward), 114 W m^{-2} , on average, over the course of the year when the skies are clear (Table 1).

The presence of clouds decreases the net amount of radiation absorbed by the surface. Although all of the hourly mean LW CRFs for all types of cloud conditions exceed 10 W m^{-2} at all times of the day (Fig. 5b), the magnitudes of negative SW CRFs (Fig. 5c) during the daylight can be up to 4 times larger than their LW counterparts, resulting in negative NET CRF (Fig. 5d). Overall, clouds deplete the amount of surface insolation more than they add to the downwelling LW flux

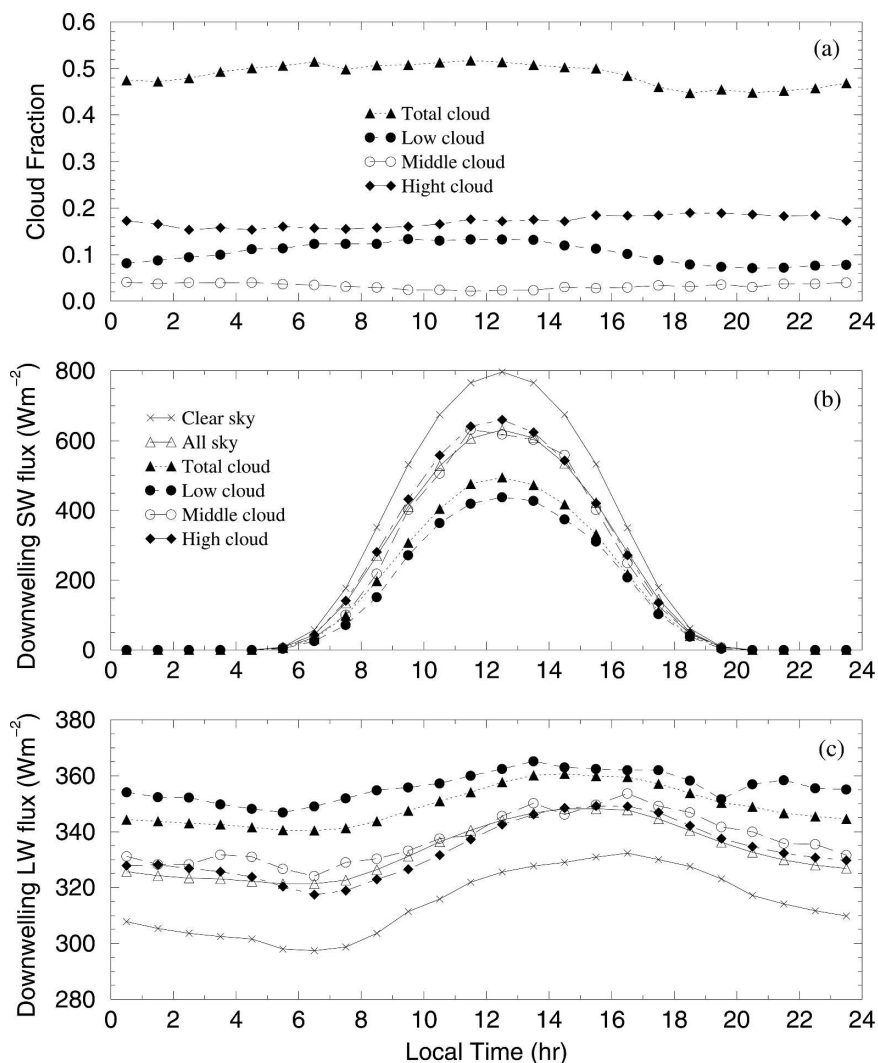


FIG. 4. Same as Fig. 1, except for hourly means.

resulting in a NET total-cloud forcing of -37 W m^{-2} (Table 1). The NET CRFs under different sky conditions are mainly determined by their SW CRFs during daytime, and entirely by their LW CRFs during the night. Low clouds have the largest cooling effect during the day and greatest warming effect during the night, and a strong net cooling effect on the surface. High clouds have the least warming effect during the night and cooling effect during the day with a weak net cooling effect on the surface. Combining these surface CRFs with TOA CRFs will allow us to determine if clouds are warming or cooling the atmosphere in a future study.

4. Comparisons with other datasets

The monthly means of C_T (Fig. 1a) are compared in Fig. 6 with the averages of surface observations re-

ported by Warren et al. (1986) and Lazarus et al. (2000), and the analyses of imagery from the eighth *Geostationary Operational Environmental Satellite (GOES-8)* over the SCF (Khayer et al. 2002). Monthly means of C_T derived from Warren et al. (1986) were averaged from 11 yr of surface observations taken between January 1971 and December 1981 within a 5° region centered near the SCF. Lazarus et al. (2000) averaged surface observations taken during a 10-yr period from December 1981 to November 1991 at two stations, Oklahoma City, Oklahoma, and Wichita, Kansas, near the SCF. The *GOES-8* results were derived from half-hourly, 4-km radiances taken by *GOES-8* daytime observations using the layer bispectral threshold method (LBTM; see Minnis et al. 1995) over an area of $0.3^\circ \times 0.3^\circ$ centered on the SCF for the same period as this study. As shown in Fig. 6 and summarized in

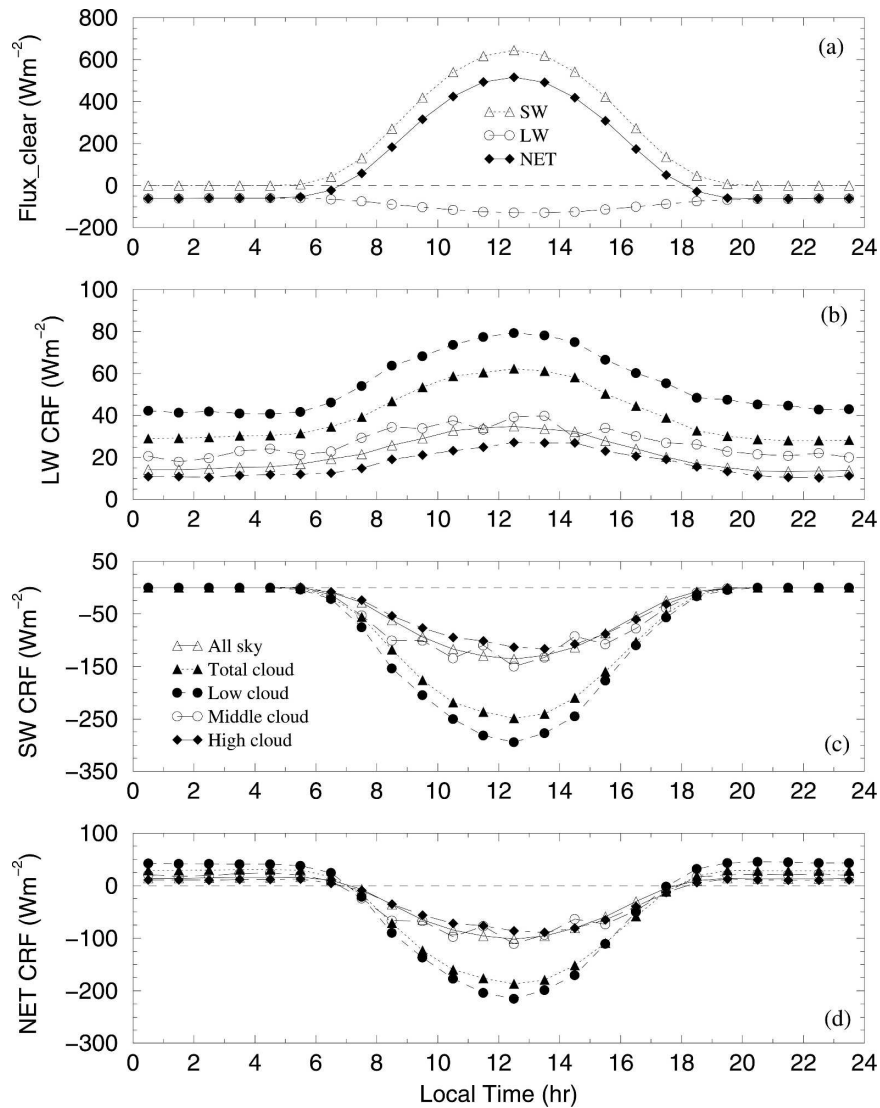


FIG. 5. Same as Fig. 2, except for hourly means.

Table 2, the monthly means of C_T from four studies agree very well in general trend and magnitude with almost identical annual averages. Similar results were found by Lazarus et al. (2000) using 8 yr (1983–91) of C2 data from the ISCCP. Although the monthly means from the various datasets are not exactly the same, they all show that cloud cover was greatest during winter and spring, least during summer and fall, and dropped significantly from June to July.

The C_L , C_M , and C_H means in Table 2 from the surface observations are much larger than those in this study. This discrepancy is mainly due to differences in the definitions of low, middle, and high clouds between this study and the surface data. Herein, the objective is to study the impact of single-layer clouds on the SRB, whereas Warren et al. (1986) and Lazarus et al. (2000)

focused on estimating the cloud amount by including all clouds in the atmospheric column based on a given overlap assumption. As listed in Table 2, the sum of C_L , C_M , and C_H is only 63% of C_T in this study. In the Warren et al. (1986) and Lazarus et al. (2000) averages, they are 122% and 126%, respectively. The *GOES-8* layer cloud amounts are not included in Table 2 because of differences in the definitions of low and midlevel clouds. However, the satellite retrievals produced an average fractional coverage of 0.21 for clouds with tops higher than 6 km. This value is between the random overlap–corrected surface observations and the radar–lidar results and suggests that the random overlap correction may be too extreme (e.g., Hogan and Illingworth 2000).

Figure 7 compares the surface SW fluxes and CRFs

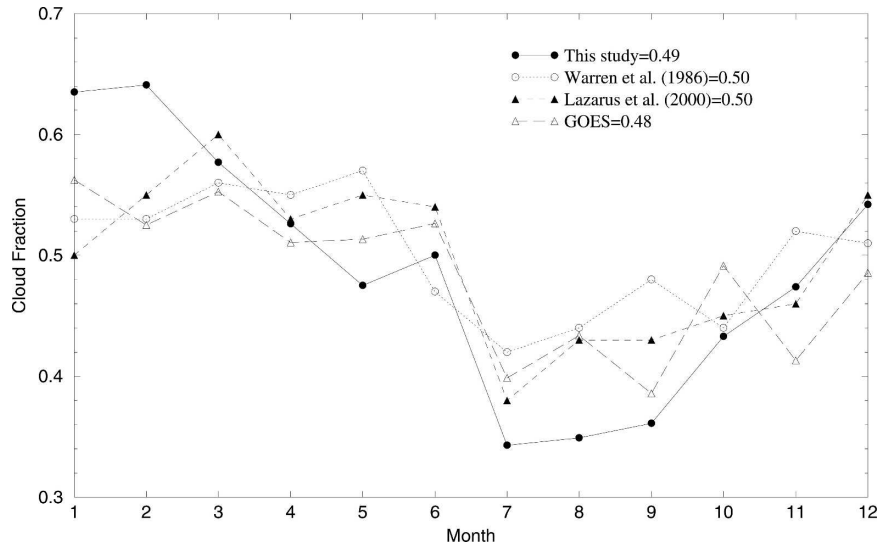


FIG. 6. Comparison of monthly mean cloud amounts from surface and satellite observations. Warren et al. (1986) means are from 1971–81 surface observations taken within a 5° region centered near the SCF. Lazarus et al. (2000) results derived from 1981–91 data taken at Oklahoma City, OK, and Wichita, KS. GOES results are averages over an area of $0.3^\circ \times 0.3^\circ$ centered on the SCF for the same period as this study.

from this study with those from other previous research that used empirical parameterizations and satellite observations. The monthly downwelling all-sky SW fluxes (Fig. 1b) are compared with those of Gautier and Landsfeld (1997), who used *GOES-7* data taken from March 1993 through April 1994 over a $250\text{-km} \times 250\text{-km}$ area centered on the ARM SCF. The monthly downwelling all-sky SW fluxes in this study are systematically higher ($\sim 29 \text{ W m}^{-2}$) than the Gautier and Landsfeld (1997) results (Fig. 7a). This discrepancy may be due to 1) different datasets (surface versus satellite and model), 2) spatial coverage (a point versus $250 \text{ km} \times 250 \text{ km}$), and 3) time periods (6 yr from January 1997 to December 2002 versus 14 months from March 1993 to April 1994) between these two studies. The monthly clear-sky and all-sky net SW fluxes and CRFs are compared with the results of Li and Leighton (1993), which were derived from Earth Radiation Budget Experiment TOA-reflected SW fluxes taken between November

1984 and December 1989 for two $2.5^\circ \times 2.5^\circ$ boxes between 35° and 37.5°N , and longitudes 95° to 97.5°W (Li_B) and 97.5° to 100°W (Li_A). Since the SCF is located on the boundary of the Li and Leighton boxes, the ARM results are compared to the averages from both boxes. The annual averages of clear-sky and all-sky net SW fluxes from both studies agree within 6 W m^{-2} , and the CRFs in this study are between the values of the two boxes. The datasets from the two time periods track follow similar seasonal patterns except for the minimum in SW CRF found in the ARM data during April.

5. Error analysis

a. Sampling biases and clear-sky screening

The biases in data sampling and processing are potential problems in calculating CRFs from observational data. As discussed earlier, to minimize the tem-

TABLE 2. Seasonal and annual averages of cloud fraction at the ARM SCF, where D denotes this study, W denotes Warren et al. (1986), and L denotes Lazarus et al. (2000). Note that the low-, middle-, and high-cloud fractions in this study are single layers, while they are either single layers or multilayers in other studies.

	Winter	Spring	Summer	Autumn	Annual
	D/W/L	D/W/L	D/W/L	D/W/L	D/W/L
C_T (%)	60/52/54	53/56/56	40/44/45	42/48/46	49/50/50
C_L (%)	16/25/27	12/23/28	5/7/16	10/22/21	11/19/23
C_M (%)	4/11/16	4/13/15	2/12/13	4/12/14	3/12/15
C_H (%)	17/35/26	17/34/28	21/25/24	14/27/20	17/30/25

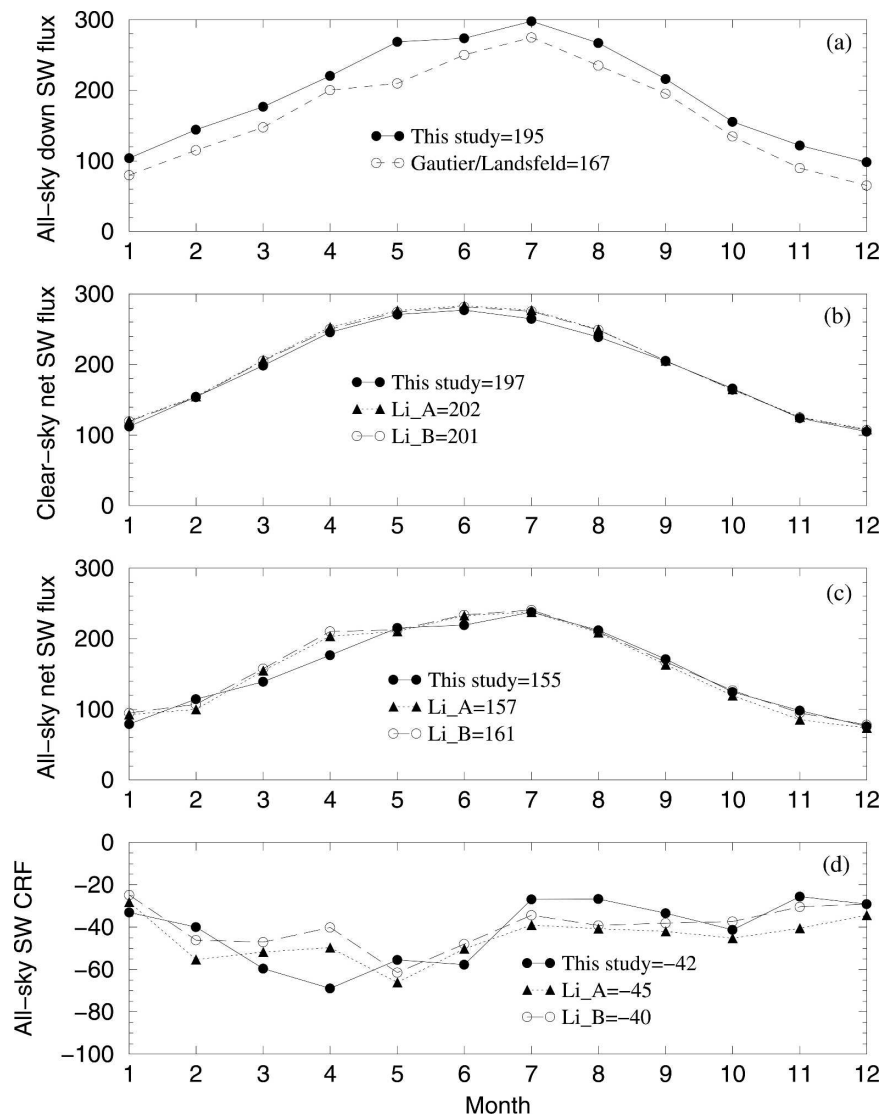


FIG. 7. Comparison of surface and satellite-derived clear- and all-sky SW fluxes and CRFs at ARM SCF. Monthly mean (a) all-sky downwelling SW flux, (b) clear-sky NET flux, (c) all-sky NET flux, and (d) all-sky CRF. Li_A results are means for ERBE data from November 1984 to December 1989 for the region between 35° – 37.5° N and 97.5° – 100° W. Li_B is the same as Li_A_x except for 95° – 97.5° W. Gautier–Landsfeld (1997) results are averages derived from *GOES-7* data taken March 1993–April 1994 over a $250 \text{ km} \times 250 \text{ km}$ area centered on the SCF.

poral sampling bias, both clear-sky and cloudy fluxes were binned and averaged in 1-h intervals, and the monthly mean clear-sky fluxes and CRFs were averaged from 24-h mean values. Imperfect cloud masking is another potential source of uncertainty in calculating CRFs because the monthly mean clear-sky fluxes can be easily contaminated by a few percent cloud cover, which would artificially increase SW CRFs and decrease LW CRFs. To minimize this problem, we used a

combination of ARM radar, lidar, and ceilometer observations to identify clear-sky conditions first and then used the ratio (>0.7) of the PSP-measured downwelling SW flux to the fitted clear-sky flux to further screen the data. Different ratio values, such as 0.8 and 0.9, provided almost the same clear-sky SW and LW fluxes as the 0.7 ratio but with fewer clear-sky samples. The annual-averaged net SW flux increases from 191.1 to 196.8 W m^{-2} , and the net LW flux decreases from -80.9 to

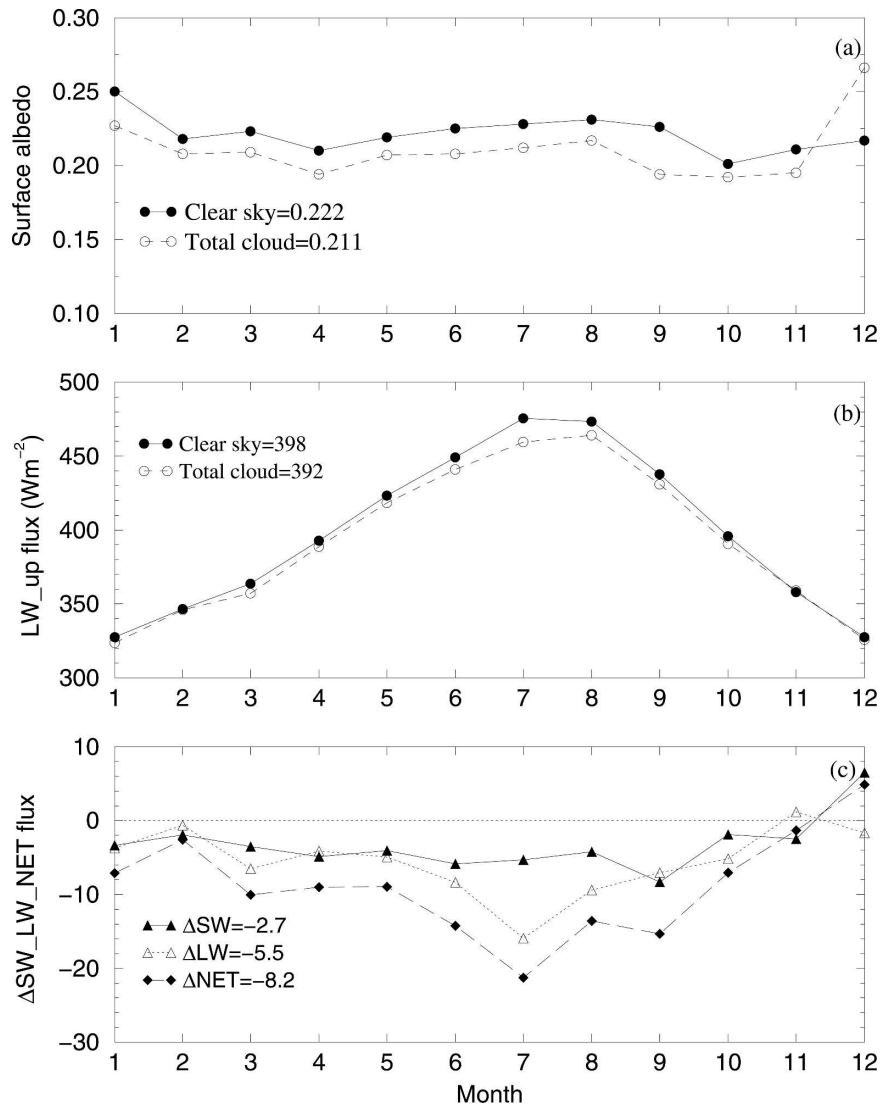


FIG. 8. Comparison of monthly mean surface radiative parameters at SFC for clear-sky and total-cloud conditions, 1997–2002. (a) Surface albedo and (b) upwelling LW flux. (c) SW, LW, and NET flux differences: $\Delta SW = SW_{\text{clear}} - SW_{\text{cloud}}$, $\Delta LW = LW_{\text{cloud}} - LW_{\text{clear}}$, and $\Delta NET = \Delta SW + \Delta LW$.

-83.1 W m^{-2} after applying the ratio test, indicating that additional cloud cover was removed from the clear-sky data.

b. The uncertainties in CRFs due to surface albedo and LW upwelling flux

In this study, the CRF is determined by the difference between the net surface fluxes with and without the presence of clouds. In fact, the CRF should be the difference between the net surface fluxes under cloudy and clear-sky conditions during cloudy periods. Since it is impossible to measure clear-sky fluxes under cloudy conditions, determination of the clear-sky values is an

other potential source of uncertainty in calculating CRF from observational data.

The monthly mean surface albedos (Fig. 8a) during clear-sky periods are normally about 0.01–0.02 higher than those for cloudy periods (except for December). Differences can arise for several reasons including the solar zenith angle (SZA) and surface moisture. Surface albedos typically increase with SZA (time from local noon), that is, they are larger during the early morning and late afternoon than at local noon. This relationship is quite apparent for clear-sky conditions because the direct SW transmission is predominant. Under cloudy conditions, the SZA dependence is greatly reduced be-

cause of the relative dominance of diffuse SW transmission (e.g., Minnis et al. 1995). During the 6-yr period, the averaged SZAs of clear-sky and cloudy periods are $\sim 65^\circ$ and 55° , respectively. Thus the larger clear-sky SZA is consistent with the higher clear-sky surface albedo as demonstrated in Fig. 8a. Increased soil moisture tends to darken a surface, reducing surface albedo (e.g., Matthias et al. 2000). During and after rain, the surface will tend to be darker than average. Except for short-lived thunderstorms, rain is normally accompanied by considerable cloud cover, and the cloud cover prevents rapid drying of the surface by decreasing the available SW flux. Thus the soil moisture should, on average, be greater during overcast conditions than under clear skies. The greater surface albedo during the cloudy period in December is mainly determined by four heavy snow periods that lasted for a few days.

The annual difference in surface albedo between clear-sky and cloudy conditions is 0.011 (or $\sim 5\%$), which results in an annual difference of -2.7 W m^{-2} [$\text{SW}_{\downarrow\text{clear}} \times (R_{\text{cloud}} - R_{\text{clear}})$]. This suggests that the altered SW CRFs would be 2.7 W m^{-2} more negative than the current values if the cloudy surface albedo was used to calculate the clear-sky-reflected SW flux, that is, the listed SW CRF values in Table 1 should be adjusted by -2.7 W m^{-2} after modification. The monthly mean upwelling LW fluxes for clear-sky and cloudy periods are illustrated in Fig. 8b, with their differences in Fig. 8c. The yearly averaged upwelling LW flux during cloudy periods is 5.5 W m^{-2} smaller than during clear skies, owing to the large difference in summer. The NET effect, the sum of SW and LW, is -8.2 W m^{-2} , indicating that the tuned NET CRFs would be 8.2 W m^{-2} more negative than the current values if the cloudy surface albedos and upwelling LW fluxes were used as clear-sky references in calculating CRFs.

c. New parameterizations

Li and Trishchenko (2001) argued that aerosols and water vapor are the main factors affecting clear-sky downwelling fluxes, with the latter dominating. To illustrate the importance of atmospheric water vapor to the downwelling SW and LW fluxes, consider Fig. 9 (clear-sky periods only). To produce Fig. 9, the downwelling SW and LW fluxes were binned and averaged in 1-cm intervals of the microwave radiometer-retrieved PWV. The differences between those fluxes and their corresponding monthly means are plotted versus PWV in Fig. 9. The NET flux is the sum of SW and LW fluxes in each 1-cm interval of PWV. Figure 9 demonstrates that the downwelling SW flux decreases and LW flux

increases with increasing PWV, and the NET flux is slightly dominated by LW flux.

To quantify the water vapor effect, the clear-sky downwelling LW and normalized SW (SW/μ_0 , the ratio of SW flux to μ_0 , the cosine of SZA) fluxes have been parameterized as a logarithmic function of PWV based on the 6-yr ARM dataset. As seen in Fig. 10, hourly mean SW/μ_0 decreases and the LW flux increases fairly smoothly with increasing PWV. The greater scattering and smaller correlation for SW flux than for the LW fluxes with PWV reflect the greater sensitivity of the SW flux to other factors, like aerosols and surface albedo, which can significantly affect the clear-sky downwelling SW flux. To assess the uncertainties in the downwelling SW and LW fluxes due to differences in PWV during clear-sky and cloudy conditions, the parameterizations (i.e., the least square fits) in Fig. 10 were applied to both clear-sky and cloudy PWVs to adjust clear-sky fluxes to compare with the measured clear-sky fluxes; the results are plotted in Fig. 11. Figure 11a shows the monthly mean clear-sky and cloudy PWVs during the 6-yr period where the clear-sky PWV is, on average, about 75% of the cloudy PWV but varies seasonally from 59% in December up to 89% in August. Figures 11b and 11c present the monthly mean measured clear-sky downwelling SW and LW fluxes (the same values as used in Figs. 1b and 1c) and the adjusted values with the parameterizations using the clear-sky and cloudy PWVs. The ΔSW and ΔLW values in Fig. 11d are the differences between the adjusted values using the cloudy and clear-sky PWVs in the parameterizations, which rules out the difference between the adjusted values using the clear-sky PWV and the measured SW fluxes. The NET effect of the cloudy water vapor is dominated by the increased LW flux.

Traditionally, CRF estimates implicitly include the extra water vapor associated with cloudy skies as part of the clouds such that CRF is due to a combination of the presence of the clouds and the altered state of the atmospheric humidity relative to the clear-sky conditions. The results in Fig. 11 show that the cloud-droplet/crystal-induced radiative forcing can be substantially different from the traditional definition because the added water vapor in cloudy atmospheres brings its own changes to the radiation balance. The changes in the fluxes (Fig. 11d) due to the extra PWV in cloudy skies relative to the fluxes for the clear-sky PWV in Fig. 11a should be referred to here as the water vapor CRF (WVCRF). The cloud droplet radiative forcing (CDCRF) can be calculated by subtracting the values in Fig. 11d from those in Fig. 2. For example, the annual-averaged CDCRF for total cloud cover should be 6.7 W m^{-2} (40 in Fig. 2a – 33.3 in Fig. 11d) for LW,

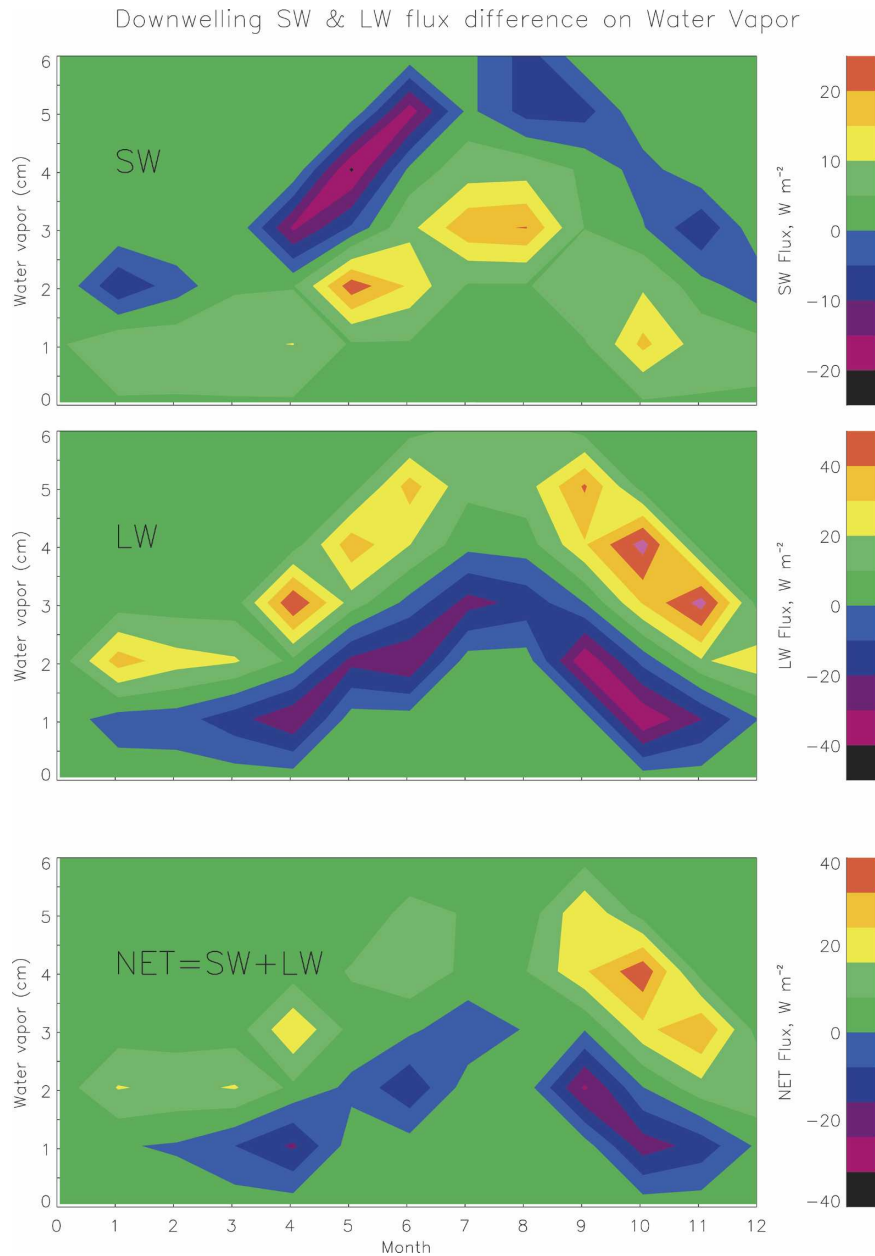


FIG. 9. Variation of individual clear-sky downwelling fluxes at SFC, 1997–2002, relative to the monthly means as functions of PWV. (a) SW, (b) LW, and (c) NET flux differences relative to the observed monthly means.

and $-69.5 W m^{-2}$ for SW. Therefore, CDCRF dominates for SW fluxes and WVCRF is dominant for LW fluxes as demonstrated in Fig. 11. The minimum in $|\Delta SW|$ during the July–August period (Fig. 11d) is due to the near saturation of the SW water vapor absorption bands in both clear and cloudy conditions. The minimum in ΔLW during the same period results from the combination of the large PWV values and the small differences between the surface temperature and effective

radiating temperature of the lower atmosphere. The annual-averaged value of ΔSW in Fig. 11d is almost the same as that reported in Figs. 6 and 7 of Li and Trishchenko (2001), who used the adding–doubling radiative transfer and the LOWTRAN-7 atmospheric transmittance models with a cloud optical depth of 40, cloud boundaries from 2 to 4 km, and PWV between 1 and 5 cm within the cloud. The excellent agreement between the observations and model simulations fur-

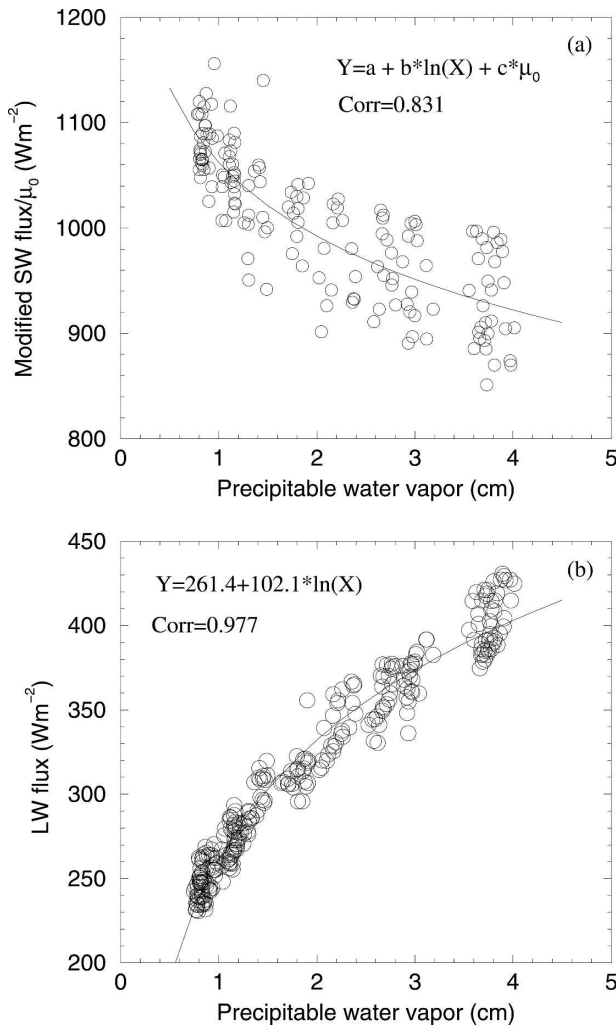


FIG. 10. Dependence of cloud-free mean downwelling fluxes on water vapor over the SFC, 1997–2002. (a) SW/μ_0 and (b) LW fluxes with fits shown as logarithmic functions of PWV. Results based on a total of 12 month \times 24 h hourly means of LW flux, and 166 (12 month \times daytime hours) hourly means of SW/μ_0 . Coefficients a , b , and c in (a) are 1062.4, -101.2 , and 0 for $\mu_0 \geq 0.5$ and 659.3, -101.2 , and 843.7 for $\mu_0 < 0.5$, respectively.

ther verify that the water vapor radiative effect is not significant for SW but is extremely important to the LW CRF.

6. Summary and conclusions

A 6-yr record of total and isolated single-layered low-, middle-, and high-cloud fractions, and their corresponding cloud radiative forcings, has been generated from ground-based measurements taken at the ARM SGP central facility between January 1997 and December 2002. This comprehensive dataset was used to examine the mean monthly and hourly variations of total,

low, middle, and high clouds and the impact of these clouds on the surface radiation budget. Additionally, we were able to explore other aspects of differences between clear-sky and cloudy-sky conditions and, for the first time, estimate their impact on surface cloud radiative forcing. From the results and comparisons with other studies, we have made the following conclusions:

- 1) At the SCF, (a) the total and single-layered low-cloud amounts are greatest during winter and least during summer; (b) single-layered high clouds occur more frequently than other types of clouds and peak during summer; and (c) single-layered midlevel clouds occur less frequently than others and have a small seasonal variation.
- 2) In overcast conditions, low clouds result in the minimum downwelling SW flux at the surface while high clouds yield the maximum SW flux. The reverse is true for their corresponding downwelling LW fluxes. The monthly mean LW CRFs for total and low clouds are greatest during the spring and fall and least during summer, and the SW CRFs are always negative with the greatest magnitudes occurring during April and the smallest during August and winter. The magnitudes of the SW and LW CRFs for other clouds are smaller than those for total and low clouds.
- 3) For the average diurnal cycle, C_T and C_L are greater in the morning and early afternoon than during late afternoon; C_H nearly mirrors C_T and C_L ; and C_M is relatively invariant. The low-cloud diurnal cycle is the most significant among the different cloud types. Despite the negative clear-sky NET flux during the nighttime hours, the daily NET flux is a positive (downward), 114 W m^{-2} , on average, over the course of the year when the skies are clear.
- 4) A detailed analysis demonstrated that the calculated CRFs do not appear to be significantly affected by uncertainties in data sampling and clear-sky screening. In the past, cloud optical properties and vertical distribution were the only factors considered when comparing modeled and observed CRF values. Cloud radiative forcing as traditionally defined includes not only the radiative impact of the hydrometeors, but also the changes in the environment. It is clear from these results that changes in the atmospheric humidity and the surface characteristics are important components of CRF. Taken together over the ARM SCF, they offset $\sim 8.2 \text{ W m}^{-2}$ or $\sim 20\%$ of the NET forcing caused by the cloud hydrometeors for the total cloud conditions in which the NET CRF is -37 W m^{-2} . The NET forcing by hydrometeors

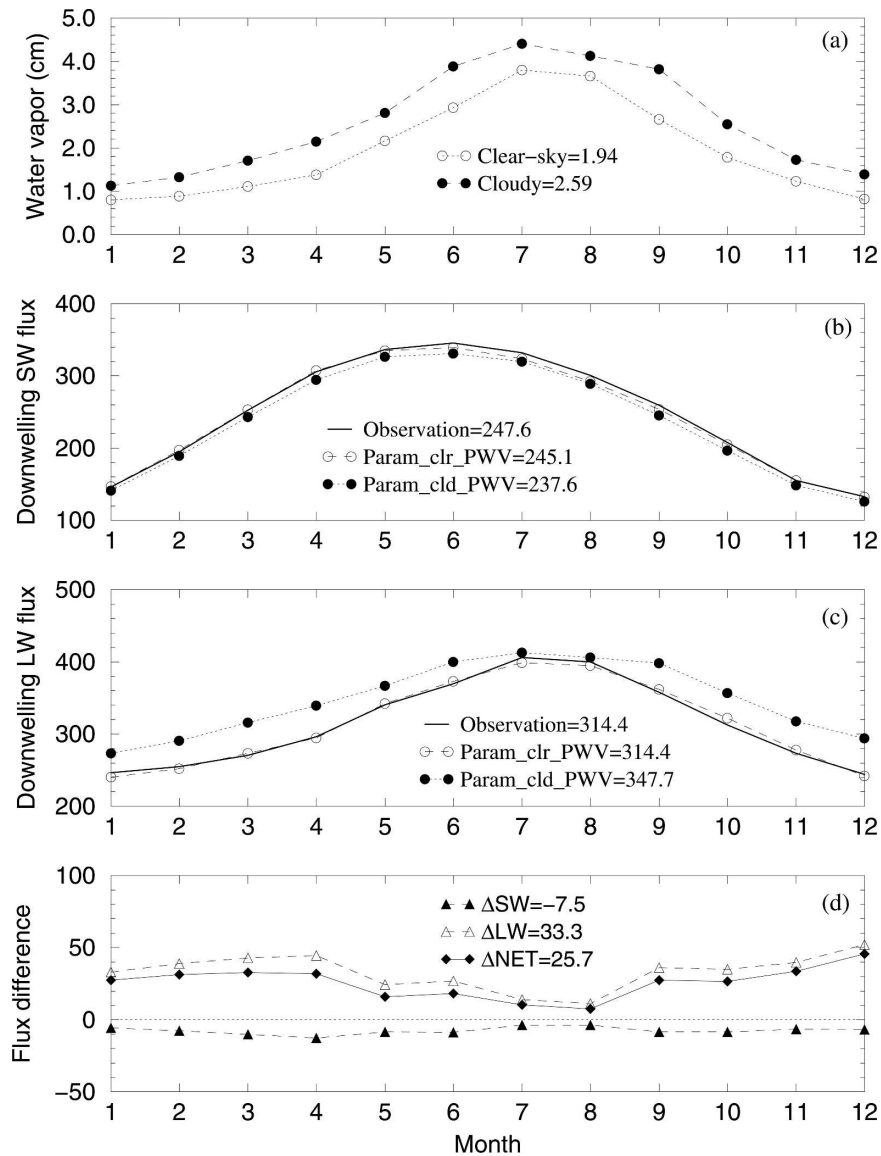


FIG. 11. Water vapor correction for monthly mean downwelling fluxes at SFC, 1997–2002. (a) Monthly mean microwave radiometer-retrieved PWV, clear-sky downwelling (b) SW and (c) LW fluxes measured by PSP and PIR (—) and calculated using formulas in Figs. 10a and 10b for clear-sky (○) and cloudy PWVs (●). (d) Flux differences, ΔSW , ΔLW , and ΔNET , between values calculated using the parameterizations in Fig. 10 with cloudy and clear-sky PWVs.

alone would be -45 W m^{-2} . Thus, modeled estimates of CRF should include the impacts of changes in humidity and surface albedo as well as those from cloud droplets and crystals.

These results can serve as a baseline for studying the radiation budget at the surface and in the atmosphere when combined with satellite measurements of the TOA fluxes and can serve as ground truth for validating satellite retrievals over the SGP site. This 6-yr dataset

over the ARM SCF should also provide statistically reliable estimates of the monthly and diurnal variations of cloud amount and radiative forcing for climate modelers to test cloud–radiation–climate interactions. The conclusions reached here apply only to the ARM SCF. Different cloud behavior and radiative impacts are expected at other locations. For example, in the Arctic, the smaller amounts of water vapor should lead to greater radiative forcing by the cloud droplets relative to that by the water vapor. In tropical locales, the op-

posite effect could occur. To better understand the geographical variability of surface cloud radiative forcing, similar analyses should be conducted using datasets collected at the ARM sites in the tropical western Pacific and in Barrow, Alaska.

Acknowledgments. Data were obtained from the Atmospheric Radiation Measurement (ARM) Program sponsored by the U.S. Department of Energy (DOE) Office of Energy Research, Office of Health and Environmental Research, Environmental Sciences Division. Special thanks to Dr. Charles N. Long at DOE PNNL for providing the Best Estimate Flux Value Added Product and some comments, to Sally Benson and Dr. Gerald G. Mace at University of Utah for providing preprocessed ARM cloud data, to Dr. Thomas P. Ackerman at DOE PNNL for providing useful suggestions and comments, to Dr. Zhanqing Li at the University of Maryland for providing the surface fluxes derived from ERBE, to Mandy Khaiyer and Dung Phan for providing the GOES-8 cloud amount averages, and two anonymous reviewers for providing insightful comments and suggestions. This research was supported by the NASA CERES project under Grant NNL04AA11G at the University of North Dakota. During this study, authors were also supported by the DOE ARM program under Interagency Agreement DE-AI02-97ER62341 and University of North Dakota Faculty Seed Funding.

REFERENCES

- Ackerman, T. P., and G. M. Stokes, 2003: The Atmospheric Radiation Measurement Program. *Phys. Today*, **56**, 38–44.
- , D. M. Flynn, and R. Marchand, 2003: Quantifying the magnitude of anomalous solar absorption. *J. Geophys. Res.*, **108**, 4273, doi:10.1029/2002JD002674.
- Barkstrom, B. R., 1984: The Earth Radiation Budget Experiment. *Bull. Amer. Meteor. Soc.*, **65**, 1170–1185.
- Cess, R. D., and Coauthors, 1990: Intercomparison and interpretation of climate feedback processes in 19 atmospheric general circulation models. *J. Geophys. Res.*, **95**, 16 601–16 615.
- , and Coauthors, 1995: Absorption of solar radiation by clouds: Observations versus models. *Science*, **267**, 496–499.
- , and Coauthors, 1996: Cloud feedback in atmospheric general circulation models: An update. *J. Geophys. Res.*, **101**, 12 791–12 794.
- Charlock, T. P., F. G. Rose, and D. A. Rutan, 2003: Validation of the archived CERES Surface and Atmospheric Radiation Budget (SARB). *Proc. 13th ARM Science Team Meeting*, Broomfield, CO, Department of Energy, 1–7. [Available online at <http://www.arm.gov/publications/proceedings/conf13/index.stm>.]
- Clothiaux, E. E., T. P. Ackerman, G. G. Mace, K. P. Moran, R. T. Marchand, M. A. Miller, and B. E. Martner, 2000: Objective determination of cloud heights and radar reflectivities using a combination of active remote sensors at the Atmospheric Radiation Measurement Program Cloud and Radiation Test Bed (ARM CART) sites. *J. Appl. Meteor.*, **39**, 645–665.
- Curry, J. A., and Coauthors, 2000: FIRE Arctic Clouds Experiment. *Bull. Amer. Meteor. Soc.*, **81**, 5–29.
- Dong, X., and G. G. Mace, 2003: Arctic stratus cloud properties and radiative forcing derived from ground-based data collected at Barrow, Alaska. *J. Climate*, **16**, 445–461.
- , P. Minnis, and B. Xi, 2005: A climatology of midlatitude continental clouds from the ARM SGP Central Facility: Part I: Low-level cloud macrophysical, microphysical, and radiative properties. *J. Climate*, **18**, 1391–1410.
- Gautier, C., and M. Landsfeld, 1997: Surface solar radiation flux and cloud radiative forcing for the Atmospheric Radiation Measurement (ARM) Southern Great Plains (SGP): A satellite, surface observations, and radiative transfer model study. *J. Atmos. Sci.*, **54**, 1289–1307.
- Gupta, S. K., D. P. Kratz, A. C. Wilber, and L. C. Nguyen, 2004: Validation of the Langley parameterized algorithms used to derive the CERES/TRMM surface radiative fluxes. *J. Atmos. Oceanic Technol.*, **21**, 742–752.
- Hogan, R. J., and A. J. Illingworth, 2000: Deriving cloud overlap statistics from radar. *Quart. J. Roy. Meteor. Soc.*, **126**, 2903–2909.
- Houghton, J. T., Y. Ding, D. J. Griggs, M. Noguer, P. J. van der Linden, X. Dai, K. Maskell, and C. A. Johnson, Eds., 2001: *Climate Change 2001: The Scientific Basis*. Cambridge University Press, 881 pp.
- Khaiyer, M. M., A. D. Rapp, P. Minnis, D. R. Doelling, W. L. Smith Jr., L. Nguyen, M. L. Nordeen, and Q. Min, 2002: Evaluation of a 5-year cloud and radiative property dataset derived from GOES-8 data over the Southern Great Plains. *Proc. 12th ARM Science Team Meeting*, St. Petersburg, FL, Department of Energy, 1–14. [Available online at <http://www.arm.gov/publications/proceedings/conf12/index.stm>.]
- Lazarus, S. M., S. K. Krueger, and G. G. Mace, 2000: A cloud climatology of the Southern Great Plains ARM CART. *J. Climate*, **13**, 1762–1775.
- Li, Z., and H. G. Leighton, 1993: Global climatologies of solar radiation budgets at the surface and in the atmosphere from 5 years of ERBA data. *J. Geophys. Res.*, **98**, 4919–4930.
- , and A. P. Trishchenko, 2001: Quantifying uncertainties in determining SW cloud radiative forcing and cloud absorption due to variability in atmospheric conditions. *J. Atmos. Sci.*, **58**, 376–389.
- Long, C. N., and T. P. Ackerman, 2000: Identification of clear skies from broadband pyranometer measurements and calculation of downwelling shortwave cloud effects. *J. Geophys. Res.*, **105**, 15 609–15 626.
- Matthias, A. D., A. Fimbres, E. E. Sano, D. F. Post, L. Accioly, A. K. Batchily, and L. G. Ferreira, 2000: Surface roughness effects on soil albedo. *Soil Sci. Soc. Amer. J.*, **64**, 1035–1041.
- Minnis, P., and E. F. Harrison, 1984: Diurnal variability of regional cloud and clear-sky radiative parameters derived from GOES data. Part III: November 1978 radiative parameters. *J. Climate Appl. Meteor.*, **23**, 1032–1052.
- , W. L. Smith Jr., D. P. Garber, J. K. Ayers, and D. R. Doelling, 1995: Cloud properties derived from GOES-7 for the spring 1994 ARM Intensive Observing Period using version 1.0 of the ARM satellite data analysis program. NASA Reference Publication 1366, 59 pp.
- Moran, K. P., B. E. Martner, M. J. Post, R. A. Kropfli, D. C. Welsh, and K. B. Widener, 1998: An unattended cloud-

- profiling radar for use in climate research. *Bull. Amer. Meteor. Soc.*, **79**, 443–455.
- Ramanathan, V., R. D. Cess, E. F. Harrison, P. Minnis, B. R. Barkstrom, E. Ahmad, and D. Hartmann, 1989: Cloud-radiative forcing and climate: Results from the Earth Radiation Budget Experiment. *Science*, **243**, 57–63.
- Rossow, W. B., and Y.-C. Zhang, 1995: Calculations of surface and top-of-atmosphere radiative fluxes from physical quantities based on ISCCP data sets, 2. Validation and first results. *J. Geophys. Res.*, **100**, 1166–1197.
- Shi, Y., and C. N. Long, 2002: Best Estimate Radiation Flux Value-Added Procedure: Algorithm operational details and explanations. DOE ARM Tech. Rep. TR-08, 51 pp. [Available online at http://www.arm.gov/publications/tech_reports/arm-tr-008.pdf.]
- Shupe, M., and J. M. Intrieri, 2004: Cloud radiative forcing of the arctic surface: The influence of cloud properties, surface albedo, and solar zenith angle. *J. Climate*, **17**, 616–628.
- Tian, B., and V. Ramanathan, 2002: Role of tropical clouds in surface and atmospheric energy budget. *J. Climate*, **15**, 296–305.
- USCCRI, cited 2001: The climate change research initiative. [Available online at www.climate-science.gov/about/ccri.htm.]
- Warren, S. G., C. J. Hahn, J. London, R. M. Chervin, and R. L. Jenne, 1986: Global distribution of total cloud cover and cloud type amounts over land. NCAR Tech. Note NCAR/TN-273+STR, National Center for Atmospheric Research, Boulder, CO, 229 pp.
- Wielicki, B. A., R. D. Cess, M. D. King, D. A. Randall, and E. F. Harrison, 1995: Mission to Planet Earth: Role of clouds and radiation in climate. *Bull. Amer. Meteor. Soc.*, **76**, 2125–2153.
- , and Coauthors, 1998: Clouds and the Earth's Radiant Energy System (CERES): Algorithm overview. *IEEE Trans. Geosci. Remote Sens.*, **36**, 1127–1141.
- Zhang, Y.-C., W. B. Rossow, and A. A. Lacis, 1995: Calculations of surface and top-of-atmosphere radiative fluxes from physical quantities based on ISCCP data sets, 1. Method and sensitivity to input data uncertainties. *J. Geophys. Res.*, **100**, 1149–1165.